Electronic structure of tin monochalcogenides from SnO to SnTe

I. Lefebvre* and M. A. Szymanski
IEMN (UMR 9929 CNRS), Avenue Poincaré, Cité Scientifique, Boîte Postale 69, 59652 Villeneuve d'Ascq Cedex, France

J. Olivier-Fourcade and J. C. Jumas
LPMC (UMR 5617 CNRS)-Université Montpellier II, place Eugene Bataillon, 34095 Montpellier Cedex 5, France
(Received 12 January 1998)

The family of tin monochalcogenides (SnX, X=O, S, Se, or Te) is calculated in order to point out trends in properties. Electronic structures are calculated from density functional theory pseudopotential and tight-binding theories. Resulting densities of states present similar features. Calculated Sn($5s$) populations and charge-density contours are shown to be consistent with the presence of a lone pair. The lone pair is also studied from Mössbauer spectroscopy, which points out the particular case of SnO. [S0163-1829(98)07427-X]

Tin monochalcogenides constitute a family of compounds that are written as SnX, X being a chalcogen (O, S, Se, or Te, which are group-VI elements). Generally, compounds belonging to a given family present similar properties that gradually change with increasing atomic number. As the best example, one may consider III-V compounds. They have the same zinc-blende crystalline structure with tetrahedral environment, the same sp^3 hybridization, and the same kind of semiconducting electronic structure. In this paper, we are interested in finding common trends and differences in electronic structure for the whole family of SnX crystals.

The electronic valence configuration is $4d^{10}5s^25p^2$ for tin atoms and ns^2np^4 for chalcogens ($n=2$, 3, 4, and 5 for O, S, Se, and Te, respectively). These atomic configurations may change with the compound due to the crystalline environment. This change is evaluated while taking bonds in the purely ionic limit, and assigning electrons to the most electronegative element of each bond, in order to obtain a net charge on atoms, which is generally called oxidation state. In SnX, the chalcogen is always the most electronegative element and will thus ''capture'' two electrons from the tin atom, giving rise to the electronic configurations ns^2np^6 for X and $4d^{10}5s^25p^0$ for Sn. Thus, the tin oxidation state is II. In this state, the two $5p$ electrons are considered to be engaged in bonds while the two $5s$ electrons constitute a lone pair. As previously shown,[1,2] this pair does not take part in the bonding but it tends to expand as far as possible, distorting the atomic arrangement around tin atoms. This is clearly shown by ^{119}Sn Mössbauer spectroscopy as the isomer shift parameter is characteristic of about 1.9 Sn($5s$) electrons and the quadrupolar splitting parameter corresponds to more or less strongly distorted environment of tin atoms. From these oxidation number considerations, one can expect that SnX compounds have similar electronic structures.

Nevertheless, their crystalline structure type are different. SnTe is clearly three dimensional whereas SnO, SnS, and SnSe are more or less layered. Only the SnSe structure may be considered as an expansion of the SnS one (an increase of the lattice parameters). From x-ray photoelectron spectra, one can separate SnO, which spectra presents four peaks, from the three other compounds, which spectra present only three peaks, within the 10 upper eV of the valence band.

Our aim here is to study similarities and differences in the electronic structures of the SnX compounds. To our knowledge, there is no study through the whole family. When a calculation is available, there is always a lack of information about quantities in which we are interested (e.g., total and partial densities of states, or electronic population). So, as we want to analyze the evolution through the family, we will use the same formalism for the calculation of a given property, even if there are some good calculations of the electronic structure for one compound or another. To perform this analysis, it is interesting to use the tin lone pair as a driving concept through three points of view: (i) Mössbauer spectroscopy, (ii) theoretical electronic populations and partial density of states gotten from tight-binding calculations, and (iii) charge-density contours gotten from density-functional theory. We will lay stress on the study of SnO because it is presently the purpose of a renewed interest, due to its ability to be an excellent anode material[5] and, up to now, there is no electronic structure that agrees with the valence-band photoemission spectrum and with the optical measurements.

In this paper, we first describe the crystalline structures, focusing on the tin neighborhood. Information on the calculation methods, tight-binding, and density-functional theory are given in Sec. II. We use both of them to analyze the tin monoxide (SnO) electronic structure in Sec. III. The electronic structure of the other three monochalcogenides is given in the following section. Finally, Sec. V is devoted to the analysis of the tin lone pair within the whole SnX family from two points of view: calculated density contours and electronic populations, and also ^{119}Sn Mössbauer spectroscopy.

I. CRYSTALLINE STRUCTURES

The structure of SnX compounds evolves from a three-dimensional one (SnTe) to a two-dimensional one (SnO) with intermediate dimension for SnS and SnSe. This intermediate behavior has been shown by an analysis of force constants from Raman and IR reflectivity measurements.[6] It can also be understood if one considers that the atomic local arrangement in SnS and SnSe are distorted structures of

TABLE I. Crystallographic data for SnX compounds.

	SnO (Ref. 7)	SnS (Ref. 8)	SnSe (Ref. 8)	SnTe (Ref. 8)
Crystal system	Tetragonal	Orthorhombic	Orthorhombic	Cubic
Symmetry space group	$P4/nmm$	$Pnma$	$Pnma$	$Fm3m$
Lattice constants (Å)	$a=3.8029$	$a=11.200$	$a=11.501$	$a=6.312$
		$b=3.987$	$b=4.153$	
	$c=4.8382$	$c=4.334$	$c=4.445$	

SnTe (see further paragraphs). The crystallographic parameters of SnX are reported in Table I. Bonds are described in Table II which displays (1) interatomic distances d, (2) the ratio $R=d/(r_i+r_j)$ where r_i is the Clementi radius of atom i. It has been shown that the main features of a given material can be recovered by considering only bonds for which R is less than 1.4.[3,4] Let us now detail the main features for each crystal.

SnTe crystallizes in the cubic NaCl structure (Fig. 1). Thus it is a three-dimensional structure. It can be considered as a close-packed arrangement of $SnTe_6$ perfect octahedra. One can point out that, in SnTe, the distance between Sn atoms is actually greater than in the other tin monochalcogenides (by an average of 0.9 Å).

The two isomorphous SnS and SnSe compounds crystallize in a structure similar to that of GeS (Fig. 2). It may be viewed as a distorted NaCl rocksalt structure in order to obtain layers made of double planes. Each plane consists of SnX zigzag chains. The gap between layers is about 1 Å (1.04 Å for SnS and 0.92 Å for SnSe). The local-atomic distribution around tin atoms is a chalcogen distorted octahedron with X-Sn-X angles slightly deviating from 90° and with three short Sn-X bonds and three long ones. Such a local atomic structure is generally found in Sn^{II} chalcogenides where the distortion is attributed to the stereochemical activity of the Sn($5s$) lone pair. From Table II, one can deduce that the layers are linked by one long Sn-X bond and two Sn-Sn bonds.

TABLE II. Interatomic distances in SnX compounds. N is the number of bonds from atom $A1$. Italic fonts stand for interlayer bonds.

Compound	$A1$-$A2$	d (Å)	N	R
SnO	Sn-O	2.23	4	1.15
	Sn-Sn	3.54	4	1.22
		3.68	*4*	1.27
	O-O	2.69	4	2.80
		4.84	*1*	5.04
SnS	Sn-S	2.63	1	1.12
		2.66	2	1.14
		3.29	2	1.41
		3.39	*1*	*1.45*
	Sn-Sn	*3.49*	*2*	1.20
	S-S	3.71	4	2.11
		3.90	*2*	2.22
SnSe	Sn-Se	2.74	1	1.10
		2.79	2	1.13
		3.34	2	1.35
		3.47	*1*	*1.40*
	Sn-Sn	*3.55*	*2*	1.22
	Se-Se	3.89	4	1.89
		3.94	*2*	1.91
SnTe	Sn-Te	3.16	6	1.18
	Sn-Sn	4.46	16	1.54
	Te-Te	4.46	16	1.81

Concerning SnO, we study here the litharge structure (isostructural with the tetragonal form of PbO). Figure 3 shows that the structure is (001) layered with a Sn-O-Sn sequence and a van der Waals gap between Sn layers (2.52 Å). Oxygen atoms are tetrahedrally bonded to Sn ones. The Sn atoms are situated at the apex of regular square-based pyramids that are based on oxygen atoms with Sn-O distances equal to 2.224 Å. This coordination is not usual for Sn^{II} atoms. Their fourfold coordination is generally derived from the distortion of an octahedral environment. In SnO, the O-Sn-O angle is of 117.3°. Let us here point out that, through the van der Waals gap, the Sn-Sn distance in SnO is nearly the same as those in SnS and SnSe, and the corresponding ratio R is less than 1.4.

II. THEORETICAL METHODS

For this study, we have used two calculation methods: first-principles density-functional theory (DFT) pseudopo-

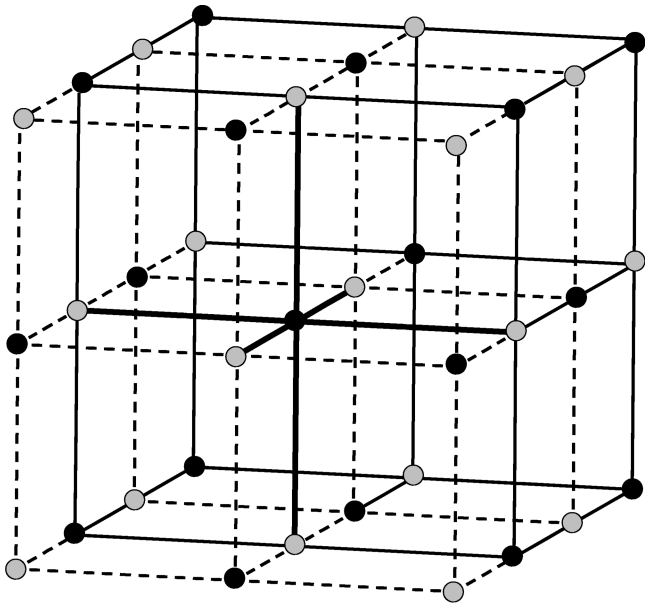

FIG. 1. SnTe atomic structure. Shaded balls stand for tellurium and bold ones stand for tin. Dotted lines correspond to bonds and bold ones represent the bonds from one tin atom.

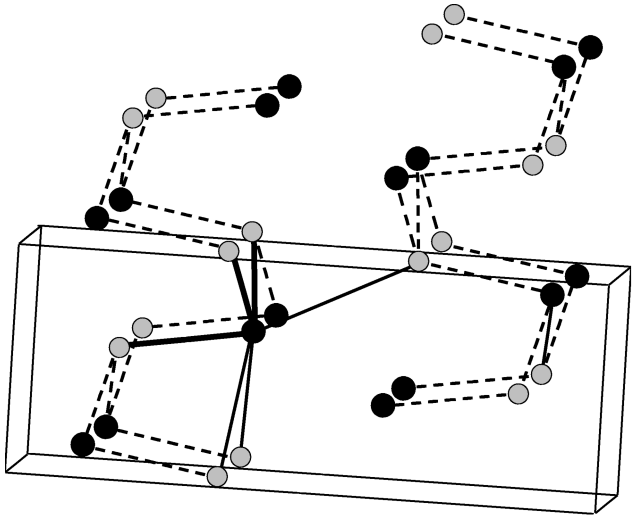

FIG. 2. SnS or SnSe atomic structure. Shaded balls stand for sulfur or selenium and bold ones stand for tin. Dotted lines correspond to bonds and bold ones represent the bonds from one tin atom.

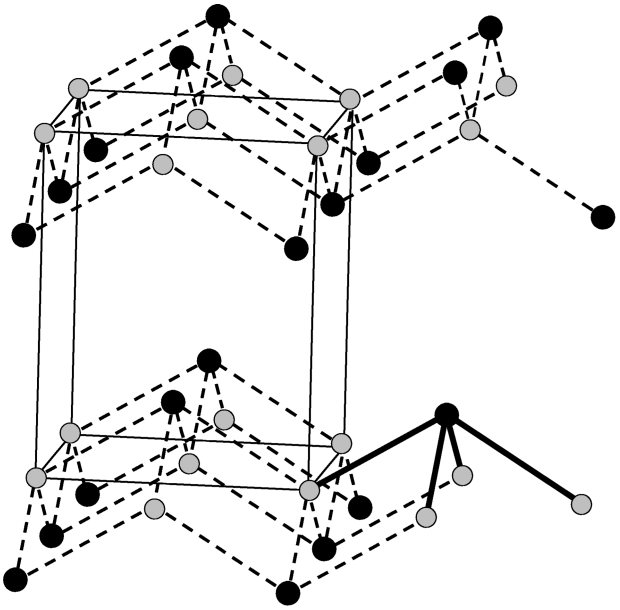

FIG. 3. SnO atomic structure. Shaded balls stand for oxygen and bold ones stand for tin. Dotted lines correspond to bonds and bold ones represent the bonds from one tin atom.

tential (CASTEP code) and empirical tight-binding. In the further paragraphs, we give brief outlines of both methods and present the advantages and drawbacks for our study.

A. First-principle technique

The first method is based on the DFT that determines the ground-state properties of an electron system by the knowledge of its electron density $\rho(\vec{r})$.[9] It allows us to map the many-electron problem on a set of one-electron equations.[10] Then, the total energy $E_T(\rho)$ of the system is written as a functional of $\rho(\vec{r})$.

In the equation that gives the functional $E_T(\rho)$ appears the exchange and correlation energy E_{xc}, which is generally not known. For purposes of practical calculations, an approximation of this term has to be introduced. The traditional one is referred to as the local-density approximation (LDA). It is based on the assumption that the relation between E_{xc} and $\rho(\vec{r})$ is locally the same as for a free-electron gas of identical density, which is quite accurately known. But in regions of low electron density, the exchange correlation is underestimated. Corrections to the LDA have been developed to correct this deficit. In particular, we use the gradient corrected LDA or generalized gradient approximation (GGA), which relates the exchange-correlation energy also to the gradient of the electron density.[11] For example, GGA typically improves the underestimation of lattice parameters in crystals. It is also well known that the reduction of E_{xc} to a simple local potential generally induces an underestimation of the energy gap. This deficiency may be corrected by the use of a ''scissor'' operator,[12] which rigidly shifts the conduction-band states to get the agreement with measured values of the band gap.

The calculation of the $E_T(\rho)$ functional also requires the use of atomic potentials. These potentials must produce the atomic core states as well as the valence states, and thus exhibit strong divergences. But, if one notices that the core states are similar in crystals to what they are in free atoms, one may replace potentials by pseudopotentials that are similar to potentials in the chemically important region beyond the core radius. In conjunction with the use of pseudopotentials, we use a plane-wave expansion for the wave function. The pseudopotentials have been generated using the optimization scheme of Lin *et al.*[13] in order to be transferrable among a variety of chemical environments, and in order to be used with a relatively small basis set (small cutoff of the plane-wave expansion).

B. Empirical technique

Empirical theories are devoted to the simulation of true energy bands by means of a restricted number of parameters. The tight-binding (TB) method can be understood as an approximate version of the linear combination of atomic orbitals (LCAO) theory. As demonstrated by the perturbation theory, the basis set consisting in free-atom states is a correct first-order basis. For practical applications the set is limited to free-atom states up to the outer shell of free-atom (minimal basis set). This ensures a proper description of valence and lowest conduction bands in crystals. Let us call $\phi_{i\alpha}$ the αth valence orbital belonging to atom i. In this basis, the energy levels E are the solutions of the secular equation $\det|H-ES|=0$ where H is the Hamiltonian matrix and S the overlap matrix. The TB approximation consists of neglecting the nondiagonal S elements. The solution of the problem requires the knowledge of the Hamiltonian matrix elements, which are

$$H_{i\alpha,i\alpha}=\langle\phi_{i\alpha}|H|\phi_{i\alpha}\rangle, \tag{1}$$

the atomic energy in the solid and

$$H_{i\alpha,j\beta}=\langle\phi_{i\alpha}|H|\phi_{j\beta}\rangle, \tag{2}$$

the hopping integrals. The Hamiltonian matrix is generally truncated in space while limiting interatomic elements to first

or second neighbors. We also make use of the two-center approximation,[14] which allows us to express each $H_{i\alpha,j\beta}$ in terms of four independant nonvanishing terms: $H_{ss}(i,j)$, $H_{s\sigma}(i,j)$, $H_{\sigma\sigma}(i,j)$, and $H_{\pi\pi}(i,j)$, where σ and π correspond to p orbitals, respectively, along or normal to the i-j bond. In order to limit the number of parameters, we use the semiempirical law:

$$H_{\alpha\beta}(i,j)=\eta_{\alpha\beta}\frac{\hbar^2}{m}\frac{1}{\Delta^2}\exp\left[-2.5\left(\frac{d}{\Delta}-1\right)\right], \tag{3}$$

where d is the interactomic distance, Δ is the reference distance depending on the concerned atomic types, and $\eta_{\alpha\beta}$ are empirically determined coefficients. Their values are chosen to reproduce the relative strength of interaction $\alpha\beta$ and are[15]

$$\eta_{ss}=-1.32,\quad \eta_{s\sigma}=1.42,\quad \eta_{\sigma\sigma}=2.22,\quad \eta_{\pi\pi}=-0.63. \tag{4}$$

The law (3) has been successfully used to calculate the electronic structure of many tin compounds,[2] chalcogenides,[1,3] and oxides,[4] and is thus particularly suited for this study.

C. Advantages and drawbacks

The main advantage of the DFT-GGA-pseudopotential method is to be first principles. As the electronic density $\rho(\vec{r})$ is calculated, one can plot charge-density maps that are useful to study the Sn($5s$) lone-pair location and its activity on the tin environment. It is much more computer time consuming than TB. However, its main drawback is that it does not provide a clear understanding of bonding. This is not the case of tight binding where the importance of each bond is given by the value of each $H_{i\alpha,j\beta}$ term. Another advantage of the TB method is that the coefficients of LCAO expression of the crystal waves are known. Thus, one can easily derive the partial density of states (the projection of the density of states on particular atomic states) and the partial electronic population on atoms by integration of partial densities.

Taking these points into account, we adopt for this study the following approach. We begin to study SnO, for which we are particularly interested. We first calculate its electronic structure (band structure and density of states) with the *ab initio* method. Then we fit the TB parameters (atomic energies and reference distances Δ) on the *ab initio* band structure. As we want to study the evolution through the family, we transfer the analysis on the fitted SnO parameters to the three other compounds and then we are led to fit only atomic energies to get the agreement with x-ray photoemission spectroscopy (XPS). Finally, the lone-pair study uses (i) the electronic population calculated with the TB electronic structure and (ii) the electronic density contours calculated with the *ab initio* method.

III. SnO ELECTRONIC STRUCTURE

Among numerous previous studies devoted to tin oxides, one can distinguish two types: (i) those dealing with SnO_x films as melting of SnO and SnO_2, and the $SnO \rightarrow SnO_2$ oxidation process, and (ii) those studying SnO phase unstability with temperature and its dynamic properties. This material has recently presented a renewed interest for lithium batteries.[5] But most of these studies are purely experimental.

TABLE III. Equilibrium structure parameters (a and c for the cell dimension and d for the Sn-O distance) from experimental results (Ref. 7), our *ab initio* calculation (pseudopotential) and those of Ref. 19 (FP-LMTO). Numbers in parentheses indicate the error of theoretical results relative to experience.

Parameter	Experimental	Pseudopotential	FP-LMTO
a (Å)	3.803	3.730 (−1.9%)	3.797 (−0.6%)
c (Å)	4.838	4.588 (−5.2%)	4.651 (−3.9%)
d (Å)	2.224	2.204 (−0.9%)	2.203 (−0.9%)

To our knowledge, there exist only a few theoretical studies of the SnO electronic structure. Cluster-type calculations have been performed using a discrete variational method [empirical in the molecular orbital model[16] or *ab initio* LDA (Ref. 17)]. As reported in Ref. 18, a TB calculation has been performed, but results are unpublished. An *ab initio* LDA has been realized[19] using the full-potential linear muffin-tin orbital (FP-LMTO) method. As the aim of all these studies was different from ours, there is always some missing information for our study (results do not include band structure or partial density of states or electronic population or contour of valence charge density). Thus, we first calculate the electronic structure (band structure or partial density of states) with the *ab initio* method.

A. *Ab initio* electronic structure

For the DFT-pseudopotential calculation, the plane-wave expansion energy cutoff (700 eV) and the Monkhorst-Pack $\vec{k}$-point set[20] are chosen to ensure the convergence of the total energy of the system to be better than 0.2 eV. The equilibrium structure has been calculated by the minimization of total energy with respect to both ionic coordinates and the lattice vectors (i.e., the shape and size of the unit cell). The comparison between calculated and experimental data is given in Table III. It is seen that the Sn-O distance is conserved within 1% of the experimental value, the a cell parameter is less well described than in Ref. 19, but an error smaller than 2% is also accurate for the structure. Since the van der Waals interaction (dipole-dipole interaction) is a many-electron phenomenon, the error on the lattice constant c is due to the approximated exchange-correlation functional and cannot be here avoided.

From this minimum-energy structure, we have calculated the band structure shown in Fig. 4(b). It is in excellent agreement with the previous one [Fig. 4(a)].[19] Band gaps for both calculations are underestimated, which is typical for DFT theory. But the application of a scissors operator (a 1.57-eV rigid shift of the conduction bands) leads to an indirect gap Γ-M of 0.2 eV, and a direct gap at M (2.64 eV) in good agreement with the experimental value from optical absorption (2.5–3.0 eV).[21]

We also calculate the density of states (DOS). The main features of the valence-band DOS are one peak at low energies [corresponding to O($2s$) states as further shown by TB] and four peaks at higher energies. The latter are shown in Fig. 5, which also presents the x-ray photoemission spectrum[16] and the previous FP-LMTO results. The distance between peaks is reported in Table IV. Our DFT valence

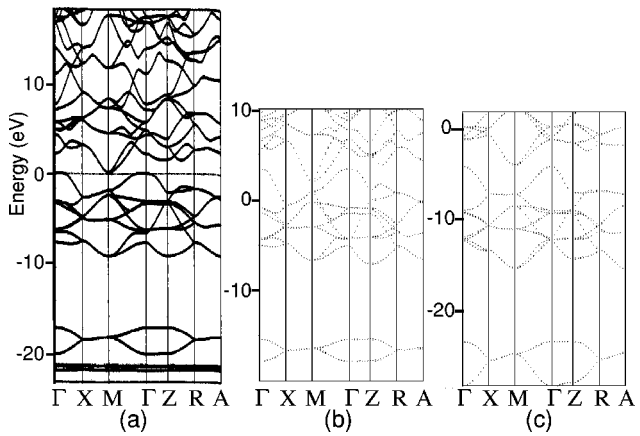

FIG. 4. SnO band structure (a) from FP-LMTO (Ref. 19), (b) from our LDA calculation, and (c) from the TB fit. The origins of energies are chosen differently on the three graphs, but the scale is the same.

band is broader than the experimental photoemission spectrum by 0.5 eV. The height of peak I seems to be underestimated but, as shown later by tight-binding calculations, this can be corrected by photoemission cross section. The sharp structure (between -8 and -10 eV) above peak I is also well reproduced.

B. Tight-binding electronic structure

As the XPS spectrum and our DFT density of states compare well, the *ab initio* band structure is valid (after the application of the 1.57-eV scissors operator). Thus, we now have to fit TB parameters (μ_i) in order to correctly reproduce this band structure (energies $E^{DFT}_{\vec{k},n}$ at point $\vec{k}$ and band n). To measure the ''distance'' between both, we have defined the following function:

$$\chi^2(\mu_1,\ldots,\mu_f)=\frac{1}{l_{\vec{k}}l_n}\sum_{\vec{k},n}[E^{TB}_{\vec{k},n}(\mu_1,\ldots,\mu_f)-E^{DFT}_{\vec{k},n}]^2, \tag{5}$$

where $l_{\vec{k}}$ is the number of $\vec{k}$ points and l_n is the number of bands for which the energy values $E^{TB}_{\vec{k},n}(\mu_1,\ldots,\mu_f)$ and $E^{DFT}_{\vec{k},n}$ are compared. Thus, the function $\chi^2(\mu_1,\ldots,\mu_f)$ is a measure of average square distance between tight-binding and DFT-pseudopotential band structures, calculated over a finite number of $\vec{k}$ points. The $\vec{k}$ points are chosen to be high-symmetry points of the irreducible Brillouin zone. In our calculations, the sum in Eq. (5) runs over all valence bands and two lowest conduction bands. The best set of tight-binding parameters $\mu_1,\ldots,\mu_f$ can be found by minimization of $\chi^2(\mu_1,\ldots,\mu_f)$. This has been done here by the use of the steepest descent method. However, there might exist some local minima of function $\chi^2(\mu_1,\ldots,\mu_f)$ and initial values of μ_i have to be carefully chosen. There are two kind of μ_i: (i) the atomic energies [Eq. (1)], which initial values are taken from Herman and Skillman's Hartree-Fock calculations[22] and (ii) the reference distance Δ, which is taken as the sum of the concerned atomic radii,[23] usually close to the interatomic distance. In TB, we have also to decide which neighbors to take into account (first, second, etc.). For complex structure compounds[1,2] we make use of a cutoff parameter that is empirically defined to be 1.4 times the sum of atomic radii. Thus we have here to include in the calculation Sn-O, Sn-Sn intralayer and interlayer bonding. But, as the case of oxides is particular,[4] we also include intralayer O-O bonds.

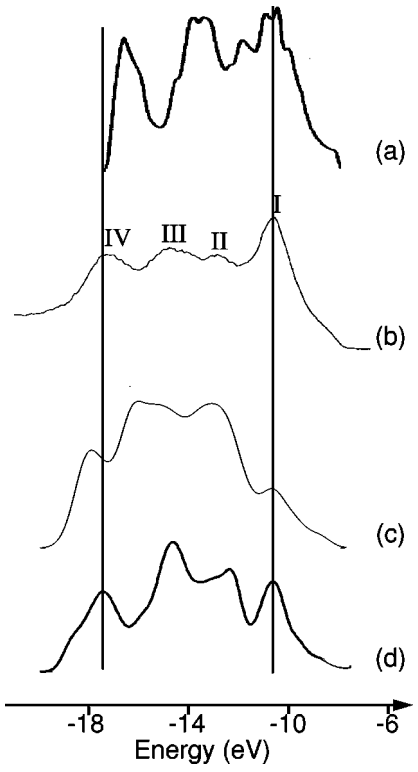

FIG. 5. SnO densities of states (a) from FP-LMTO (Ref. 19), (b) XPS spectrum, (c) from our LDA calculation, and (d) from the TB fit. They are drawn on the same energy scale and the highest-energy peak of each one are aligned.

TABLE IV. Distance (in electronvolts) between peaks in XPS spectrum, our DFT and TB calculations of SnO densities of states.

	XPS	DFT	TB
I-II	2.3	2.4	1.9
I-III	4.2	4.9	4.2
I-IV	6.7	7.2	6.7

With this first set of parameters ($\chi=0.51$ eV), the TB model is unable to reproduce the shape of lowest conduction bands and band-gap energy. If we impose the right value of direct band gap at point M, the conduction and valence bands cross during minimization of χ^2 and the material turns into a metal. A great improvement is achieved by distinguishing between the atomic orbitals energies for p states $E_{x,y}$ and E_z. This second choice of parameters ($\chi=0.41$ eV) leads to values reported in Table V. It can reproduce the shape of both valence and conduction bands. The direct band gap occurs for the Γ point and the band gap for the M point is slightly bigger. DFT calculations show just the opposite trend. But the overall description of the band structure is much better than for the first set of parameters. The impor-

TABLE V. Tight-binding parameters. Numbers in parentheses give the differences between parameters used in this work and the Hartree-Fock values. For SnO, the Ep_z value is 2.86 eV higher than the other E_p energies.

SnX	Sn			X		
	E_s (eV)	E_p (eV)	Radius (Å)	E_s (eV)	E_p (eV)	Radius (Å)
SnO	−14.85	−5.94	1.29	−27.33	−12.50	0.48
	(−2.35)	(0.0)	(−0.16)	(+1.8)	(+1.6)	(0.00)
SnS	−14.00	−5.94	1.29	−19.80	−9.27	0.88
	(−1.5)	(0.0)	(−0.16)	(+1.0)	(+1.0)	(0.00)
SnSe	−13.6	−5.94	1.29	−19.32	−8.33	1.03
	(−1.1)	(0.0)	(−0.16)	(+1.0)	(+0.8)	(0.00)
SnTe	−13.20	−5.94	1.29	−17.51	−8.50	1.23
	(−0.7)	(0.0)	(−0.16)	(−0.4)	(0.0)	(0.00)

tant difference between Sn($5p$) energies ($E_z - E_{x,y} = 2.86$ eV) seems to be related to some influence of interlayer van der Waals interactions.

The fitted tight-binding band structure is shown in Fig. 4(c). The width of the lowest band (below −20 eV on the TB results) is larger than in other calculations. As it mainly comes from O($2s$) states, this may be due to an overestimation of the O($2s$)-O($2s$) interaction. It could be fitted, but this band is not useful for our study. The value of direct band gap at the M point is 2.9 eV and at the Γ point is 3.0 eV. The value of the indirect band-gap is 0.2 eV. The band gap at the Γ point seems to be underestimated by 1.0 eV, which is mainly due to the shape of the conduction band, while the direct gap at the M point and the indirect band gap are correct. This description of the band structure is completely satisfactory for our purposes. The corresponding DOS and partial DOS are shown in Figs. 5 and 6. The four peaks are fairly well reproduced and their spacings are in better agreement with experiment than those from *ab initio* calculations (Table IV). The partial densities indicate that these peaks are mainly derived from Sn($5s$) and O($2p$) states. The contribution of Sn($5p$) states is very small. Peculiarly, peaks I and IV correspond, respectively, to the antibonding and bonding interaction between Sn($5s$) and O($2p$) states. As the photoemission cross section of the Sn($5s$) states is higher than the others, these latter peak heights will be enhanced, leading to a much better agreement between the TB density of states and the XPS spectrum.

Let us here emphasize that this TB study allows us to point out that (i) the intralayer Sn-Sn bonding leads to the indirect gap, (ii) the interlayer Sn-Sn bonding leads to the right value of band gap, to the right shape of the upper valence bands, and to the sharp structure above peak I and (iii) the intralayer O-O interactions have a strong influence on the position of peak II relative to peak I.

IV. SnX (X=S,Se,Te) ELECTRONIC STRUCTURE

We want here to analyze the evolution of the electronic structures of SnX (X=S,Se,Te) relative to the previous study of SnO. We use an alternative approach for finding tight-binding parameters. It consists of the transfer of results obtained for SnO: (i) same Sn atomic radius, (ii) Clementi atomic radius[23] for the chalcogen atom, and (iii) same kind of bonding taken into account. This last point corresponds to six Sn-X bonds and two Sn-Sn for SnS and SnSe. For SnTe, the Sn-Sn distance is 1 Å greater and the corresponding Sn-Sn interactions can be neglected. By the fitting of the remaining parameters, i.e., atomic energies, to reproduce the photoemission spectrum, we have obtained the parameter values reported in Table V. One may observe the continuous increase in differences between Herman-Skillman and fitted values from SnTe to SnO.

The SnX XPS spectra are reported in Fig. 7. In each spec-

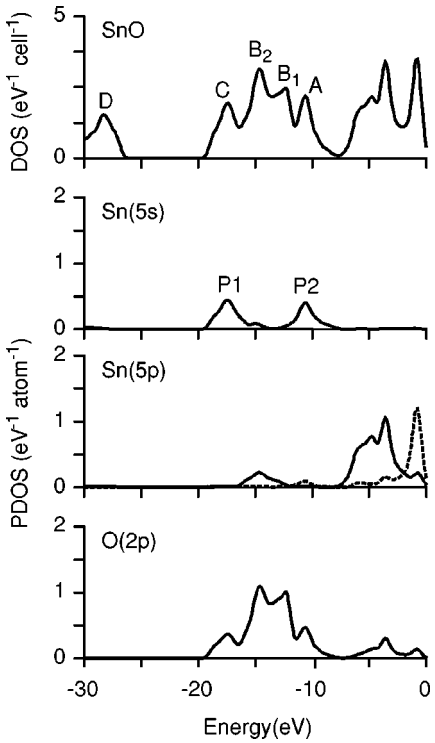

FIG. 6. SnO partial densities of states from the TB fit. Notice for Sn($5p$) that the full line corresponds to $p_{x,y}$ and the dashed one to p_z.

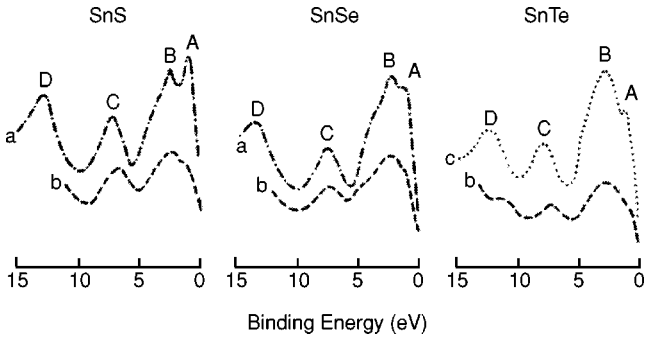

FIG. 7. Experimental photoemission data for SnX (X=S,Se,Te) compounds. (a) refers to data by Kemeny *et al.* (Ref. 24), (b) to spectra by Shalvoy *et al.* (Ref. 25), and (c) to data by Kemeny and Cardona (Ref. 26).

trum, four main peaks (labeled A, B, C, and D) can be distinguished. The spacing between peaks and even the height of the peaks are similar. This can be related to the similar local environment of tin atom in the three compounds (six chalcogen atoms) and to the same valence electron configuration for sulfur, selenium, and tellurium, consisting of two s and four p valence electrons. The calculated total and partial DOS are shown in Figs. 8, 9, and 10. The lowest energy peak D is mainly $X(s)$ type, as for SnO. Peaks A and C correspond, respectively, to antibonding and bonding interactions between Sn($5s$) and $X(p)$ states. In this way, they are similar in character to peaks labeled I and IV on the SnO density. The main difference is in peak B, which comes from interactions between Sn($5p$) and $X(p)$ states, with an important Sn($5p$) component, contrary to peaks II and III in SnO.

As for SnO, the inclusion of Sn-Sn bonds influences the shape of the highest valence band and the lowest conduction one, which is essential for an accurate description of band gaps. There is a good agreement between experimental and theoretical values (Table VI). It can be noted that the direct band-gap value decreases through the family of SnX compounds but the behavior of the indirect one is varied.

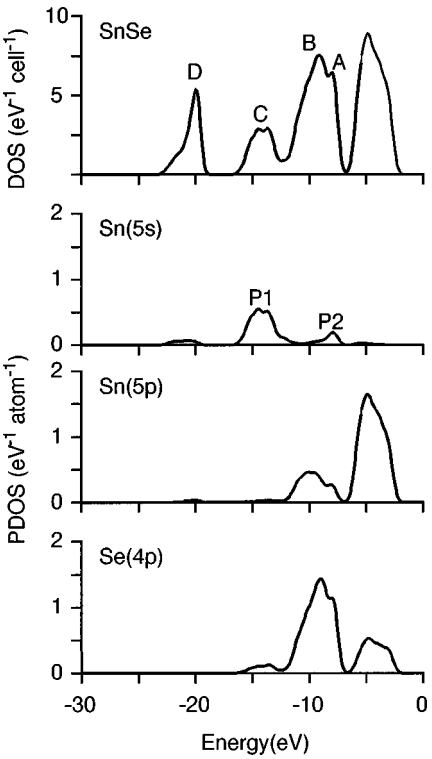

FIG. 9. SnSe total and partial DOS from the TB fit.

V. Sn($5s$) LONE PAIR

As emphasized in the Introduction, the tin oxidation state in monochalcogenide compounds is II. The Sn^{II} atoms are

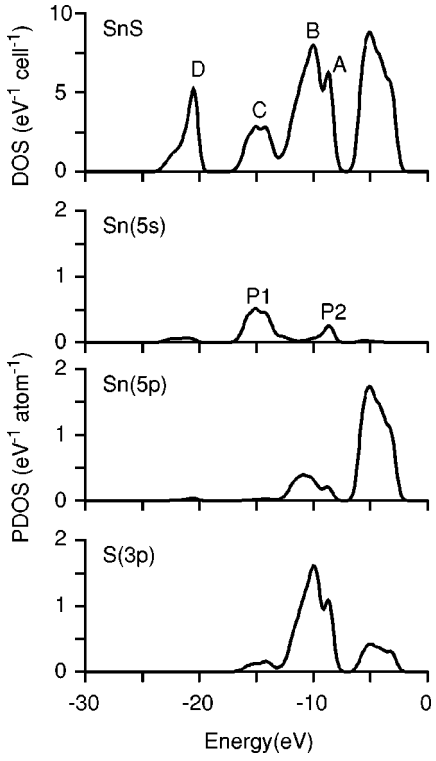

FIG. 8. SnS total and partial DOS from the TB fit.

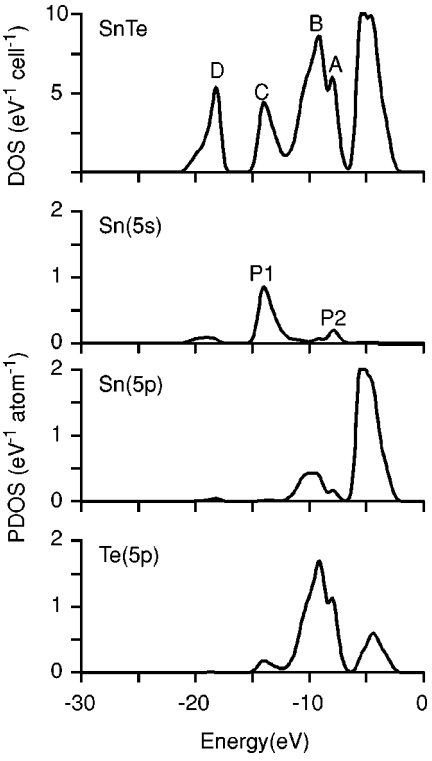

FIG. 10. SnTe total and partial DOS from the TB fit.

TABLE VI. Tight-binding and experimental values of band gaps for SnX (X=S, Se, Te) compounds.

SnX		Direct band gap	Indirect band gap	Reference
SnO	TB	2.9 eV	0.2 eV	this work
	Expt.	3.0 eV		Ref. 21
SnS	TB	2.1 eV	1.5 eV	this work
	Expt.		1.41 eV	Ref. 27
SnSe	TB	1.3 eV	0.9 eV	this work
	Expt.	1.27 eV	0.89 eV	Ref. 28
SnTe	TB	1.1 eV		this work
	Expt.			

characterized by a lone pair $5s^2$ as their atomic configuration is defined as $4d^{10}5s^25p^0$. Let us first recall the stereochemical activity notion. As we are confident in our theoretical electronic structures, we use them to study the Sn($5s$) activity. In the last part, results are analyzed in correlation with the experimental point of view through ^{119}Sn Mössbauer spectra.

A. Stereochemical activity

In oxidation state II, the Sn($5s$) electrons do not take part in the bonding, but their properties (electronic behavior, spatial occupation) are directly correlated to the Sn coordination and to the structural packing. Galy *et al.*[29] define this lone pair as an intermediate state between an inert spherical s^2-type orbital that is centered on the nucleus and a nonbonded hybridized-orbital lobe that is not spherical but localized far from the atomic nucleus. Thus, the valence shell electronic pair repulsion[30] theory takes this spatial effect into account to predict local environment symmetries. This effect is named the lone-pair ''stereochemical activity.'' In the SnX family, the local environment of a tin atom is different in type, number, and arrangement of neighbors. One may thus expect differences in the tin lone-pair activity on which we now focus.

First, we have to make sure that there is a lone pair. This is clear from Table VII where partial densities have been integrated on the valence band. The Sn($5s$) population is always greater than 1.9 electron and really constitute a pair.[2] It comes from a two-peak density of states ($P1$ and $P2$). In all cases, $P1$ corresponds to bonding states and $P2$ to antibonding ones. As both lie in the valence band, one considers that these states do not directly participate to the bonding and

TABLE VII. Tin electronic $5s$ (N_s) and $5p$ (N_p) population from tight-binding results.

	N_s	N_p
SnO	1.9355	0.8901
SnS	1.9527	1.2796
SnSe	1.9400	1.5468
SnTe	1.9696	1.2806

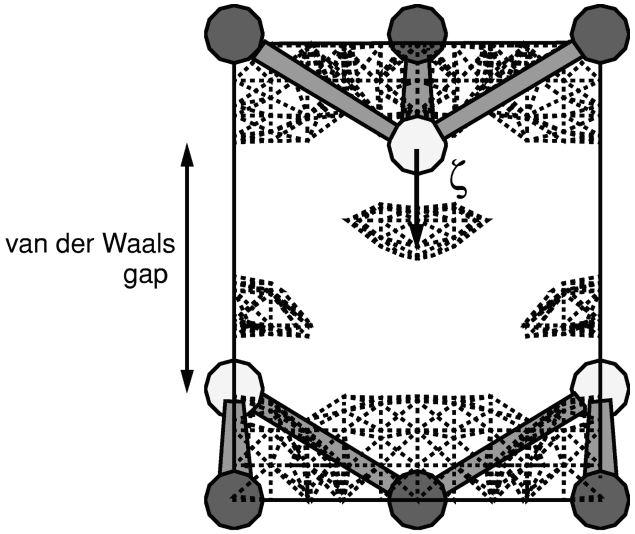

FIG. 11. Charge-density map of SnO from *ab initio* results.

the two Sn($5s$) electrons are lone. The distance between $P1$ and $P2$ is increased from SnTe to SnO. Considering these density shapes and states compositions, the case of SnO is distinct from the other three compounds. For SnO, $P1$ and $P2$ heights are similar. The related total density peaks (C and A) have nearly the same proportion of Sn($5s$) and O($2p$) characters. For the other SnX compounds, peak C is rather 30%Sn($5p$)+70%X(p). This indicates that the lone pair in SnO may have a particular behavior.

Another way to study the stereochemical activity of the Sn lone pair is to visualize the charge density around tin atoms. This may easily be realized from the calculation of the electronic charge density $\rho(\vec{r})$ (Sec. II A) for each SnX compound in the DFT formalism (Sec. II A). They are mapped in Figs. 11, 12, and 13. For SnO, a part of the electronic charge is concentrated near tin atoms. This may be interpreted to be the lone-pair density. Let us now consider the vector joining a tin nucleus to the center (highest density) of its associated lone pair. This vector is used in the elec-

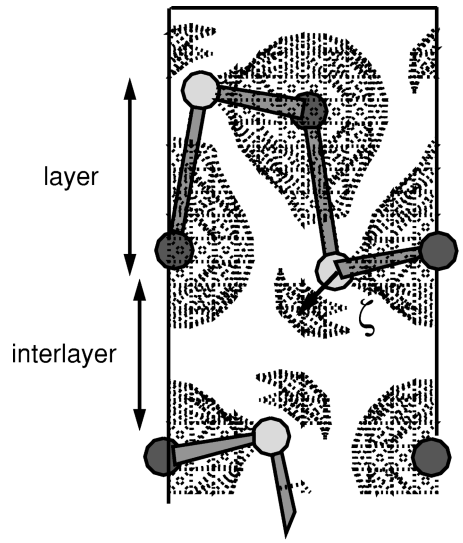

FIG. 12. Charge-density map of SnS from *ab initio* results. The map is similar to SnSe.

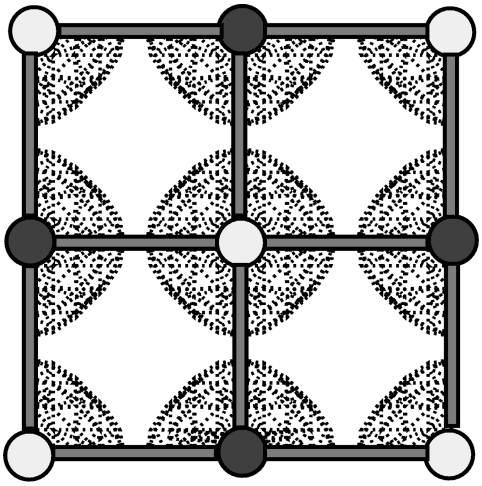

FIG. 13. Charge-density map of SnTe from *ab initio* results.

tronic lone pair localization (ELPL) model.[31] The model considers the crystal as ionic with spherical nonrecovering charge distribution and it approximates lone pairs to point charges. This leads to electric dipolar momentum $q\vec{\zeta}$ for ion possessing a lone pair with the lone-pair charge $q=-2|e|$ and $\vec{\zeta}$ the above mentioned vector. Figure 11 shows that the vector is perpendicular to the layers, directed toward the van der Waals gap. Its modulus is 0.9 Å, in excellent agreement with the one calculated by LeBellac *et al.*[32] using the ELPL model (0.903 Å). A lone pair is also observed in the SnS and SnSe case (Fig. 12). One notices that their $\vec{\zeta}$ vector is tilted relatively to the normal to the layer. This tilt lowers the dipole-dipole interaction that may be the origin of the interlayer distance (from 2.52 Å for SnO to nearly 1 Å for SnS and SnSe). On the contrary, for SnTe (Fig. 13), the electronic charge is spherically centered on atoms, in agreement with their symmetrical environment.

B. Mössbauer results

The Mössbauer spectroscopy allows the study of solids on an atomic scale and is often used to study the oxidation state and the lone-pair behavior. It can be defined as a resonant absorption spectroscopy of a γ ray between a reference material (source) and the measured compound (absorber). The change in transition energy is due to the electrostatic interaction of the nuclear charge distribution with the electronic distribution around probe atoms. Spectra are mainly characterized by two parameters: the isomer shift (δ) and the quadrupolar splitting (ΔE_Q). The first one corresponds to the peak position on the spectrum. It may be written as

$$\delta=\mathcal{N}[|\Psi_a(0)|^2-|\Psi_s(0)|^2], \tag{6}$$

where $\mathcal{N}$ is a nuclear prefactor and $|\Psi(0)|^2$ reflects the electronic density at the probe nucleus. As detailed further, this density can be considered as proportional to the Sn(5*s*) electrons in the valence band. The second parameter corresponds to the peak splitting. This splitting is induced by the electric-field-gradient and thus to the local environment distortion. It is given by

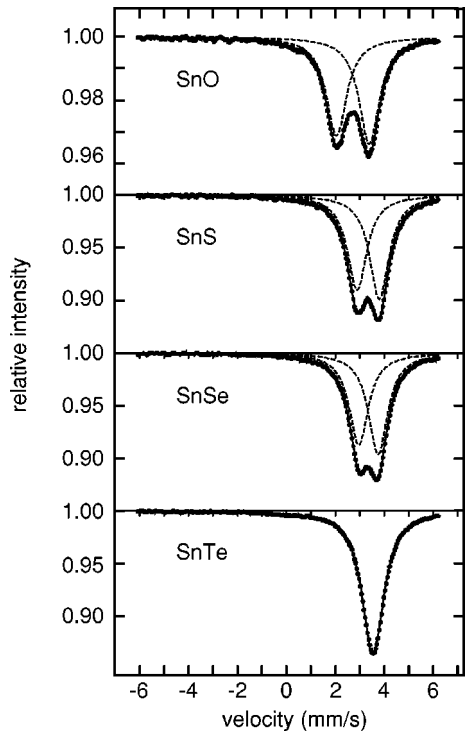

FIG. 14. Mössbauer spectra of Sn*X* compounds.

$$\Delta E_Q=\frac{eQV_{zz}}{2}\left(1+\frac{\eta^2}{3}\right), \quad \eta=\frac{V_{xx}-V_{yy}}{V_{zz}}, \tag{7}$$

where Q is the nuclear quadrupole moment of the nucleus in the excited state, e is the charge of the electron, and V_{ii} are the electric-field-gradient components in the system of the principal axis in which the tensor is diagonal. The analysis of ΔE_Q leads to a picture of the symmetry of the electron distribution close to the nucleus.

We have recorded the ^{119}Sn Mössbauer spectra for the monochalcogenides in the constant acceleration mode on a ELSCINT-AME40 spectrometer using $Ba^{119}SnO_3$ as the γ-ray source. They are shown in Fig. 14 and the related parameters are reported in Table VIII. Their values are in good agreement with previous data.[33] For Sn in the oxidation state II, one generally expects values of δ to be greater than 3 mm/s. This is not the case for SnO, where δ is at the Sn^{II} limit, similar to the β-tin one. This would be due to a greater covalency of bonding in SnO relative to those in other Sn^{II} chalcogenides. As expected, the symmetrical environment of Sn in SnTe leads to an absence of quadrupolar splitting. ΔE_Q increases with the local tin distortion, with similar values for SnSe and SnS.

TABLE VIII. Mössbauer parameters of Sn*X* (X=O,S,Se,Te) compounds at 293 K. δ is the isomer shift referred to $BaSnO_3$, ΔE_Q is the quadrupolar splitting, and Γ the linewidth at half intensity. All values are expressed in mm/s.

	δ	ΔE_Q	Γ
SnO	2.672(3)	1.335(3)	1.008(4)
SnS	3.295(2)	0.906(2)	0.961(3)
SnSe	3.308(1)	0.788(1)	0.948(3)
SnTe	3.495(1)		1.074(4)

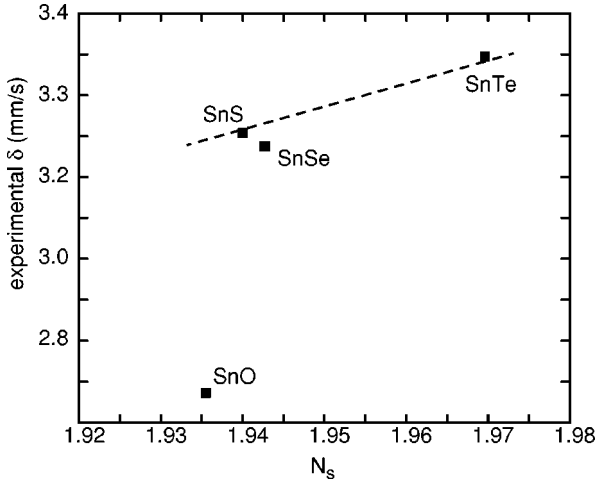

FIG. 15. Experimental Mössbauer isomer-shift vs the theoretical Sn($5s$) population. The slope of the dashed line corresponds to those deduced from law (9).

Let us now try to relate tin populations N_s and isomer shifts. The number of $5s$ electrons on the Sn nucleus $[|\Psi(0)|^2$ in Eq. (6)] can be considered in first approximation to be $N_s|\phi_0(Sn)|^2$ where $\phi_0(Sn)$ is a Slater-type orbital $[|\phi_0(Sn)|^2=17.64$ a.u.$^{-3}$ (Ref. 34)]. Combining this approximation to the detailed expression of the nuclear prefactor $\mathcal{N}$, Eq. (6) leads to (in SI units):

$$\delta=S(Z)\frac{1}{5\epsilon_0}Ze^2R_{eff}^2\left(\frac{\Delta R}{R}\right)|\phi_0(Sn)|^2(N_{s,a}-N_{s,s}), \quad (8)$$

where $S(Z=50)=2.31$ (Ref. 35) is a factor corresponding to the relativistic effect. R_{eff}, the effective radius of the Sn nucleus, is written as $1.2A^{1/3}\times10^{-15}$ m,[36] where $A=118.69$ is the mass number. $\Delta R/R=1.34\times10^{-4}$ (Ref. 36) is a calibration constant. From the Mössbauer transition, the conversion constant is 7.97×10^{-8} eV per mm/s. Thus, the numerical expression of δ (in mm/s) is

$$\delta=2.9(N_{s,a}-N_{s,s}). \quad (9)$$

We have reported in Fig. 15 the experimental values of δ vs the theoretical Sn($5s$) population. The slope of the drawn line is that of Eq. (9). It is clear that SnTe, SnS, and SnSe are correctly predicted. The point corresponding to SnO is out of the linear dependance. To mimic experimental results, the Sn($5s$) electronic population of SnO would be

$$N_s^{\exp}=N_s^{\text{th}}(\text{SnTe})-\frac{\delta^{\exp}(\text{SnTe})-\delta^{\exp}(\text{SnO})}{2.9} \quad (10)$$

as deduced from Eq. (9). The obtained value of 1.68 eV is not coherent with the existence of a lone pair, which is known to occur (from oxidation state, density contour, or ELPL results). This may be due to the two-dimensional structure of SnO, the lone pairs occupying the van der Waals gap and interacting together.

VI. CONCLUSION

We have studied the tin monochalcogenide (SnX) electronic structure from DFT-pseudopotential and tight-binding calculations. Results show that these compounds present similar features.

(1) Their density of states is composed of a peak at low energy (D) corresponding to $X(s)$ states and a group of peaks at higher energies. The bottom (C) and top (A) peaks of this group are, respectively, due to bonding and antibonding Sn($5s$)$-X(p)$ states. The distance $A-C$ regularly increases from SnO to SnTe.

(2) Their Sn($5s$) electronic population is greater than 1.9 electron. This lone pair is characteristic of the oxidation state II, in agreement with Mössbauer spectra.

But there is a great difference in the lone-pair behavior, which separates the family in two groups: SnO on one side, SnX ($X=$S, Se, Te) on the other side. This difference mainly comes from the following.

(1) The difference in proportion of Sn($5s$) relative to $X(5p)$ character in density of states peaks C and A. This is related to the difference in behavior between p_z and $p_{x,y}$ orbitals.

(2) The lone-pair stereochemical activity. In case of SnO, the lone pair points towards the interlayer space, creating a van der Waals gap. It is less active in SnS and SnTe, pushing away tin neighbors, and thus only creating a distortion relative to the NaCl structure.

In other words, SnO, which is strongly lamellar, stands out against the other SnX compounds.

*Electronic address: ile@isen.fr

[1] I. Lefebvre, M. Lannoo, G. Allan, A. Ibanez, J. Fourcade, J. C. Jumas, and E. Beaurepaire, Phys. Rev. Lett. **59**, 2471 (1987).
[2] I. Lefebvre, M. Lannoo, J. Olivier-Fourcade, and J. C. Jumas, Phys. Rev. B **44**, 1004 (1991).
[3] I. Lefebvre, M. Lannoo, G. Allan, and L. Martinage, Phys. Rev. B **38**, 8593 (1988).
[4] S. J. Sferco, G. Allan, I. Lefebvre, M. Lannoo, E. Bergignat, and G. Hollinger, Phys. Rev. B **42**, 11 232 (1990).
[5] Y. Idota, T. Kubota, A. Matsufuji, Y. Maekawa, and T. Miyasaka, Science **276**, 1395 (1997); Chem. Eng. News **75**, 39 (1997).
[6] J. D. Wiley, W. J. Buckel, and R. L. Schmidt, Phys. Rev. B **13**, 2489 (1976); H. R. Chandrasekhar, R. G. Humphreys, U. Zwick, and M. Cardona, *ibid.* **15**, 2177 (1977).
[7] J. Pannetier and G. Denes, Acta Crystallogr., Sect. B: Struct. Crystallogr. Cryst. Chem. **36**, 2763 (1980).
[8] W. B. Pearson, *Handbook of Lattice Spacing and Structure of Metals and Alloys* (Pergamon, London, 1976), Vol. 3.
[9] P. Hohenberg and W. Kohn, Phys. Rev. **136**, B864 (1964).
[10] W. Kohn and L. J. Sham, Phys. Rev. **140**, A1133 (1965).
[11] J. P. Perdew, J. A. Chevary, S. H. Vosko, K. A. Jackson, Mark R. Pederson, D. J. Singh, and C. Fiolhais, Phys. Rev. B **46**, 6671 (1992).
[12] G. A. Baraff and M. Schulter, Phys. Rev. B **30**, 3460 (1984); M. Lannoo, M. Schulter, and L. J. Sham, *ibid.* **32**, 3890 (1984).
[13] J. S. Lin, A. Qteish, M. C. Payne, and V. Heine, Phys. Rev. B **47**, 4174 (1993).
[14] J. C. Slater and G. J. Koster, Phys. Rev. **94**, 1498 (1954).
[15] W. A. Harrison, Phys. Rev. B **24**, 5835 (1981).
[16] L. Köver, Zs. Kovács, R. Sanjinés, G. Moretti, I. Cserny, G. Margaritondo, J. Pálinkás, and H. Adachi, Surf. Interface Anal. **23**, 461 (1995).

[17] J. Terra and D. Guenzburger, Phys. Rev. B **44**, 8584 (1991).
[18] J-M. Themlin, M. Chtaib, L. Henrard, P. Lambin, J. Darville, and J-M. Gilles, Phys. Rev. B **46**, 2460 (1992).
[19] E. L. Peltzer y Blanca, A. Svane, N. E. Christensen, C. O. Rodríguez, O. M. Cappannini, and M. S. Moreno, Phys. Rev. B **48**, 15 712 (1993).
[20] H. J. Monkhorst and J. D. Pack, Phys. Rev. B **13**, 5188 (1976).
[21] J. Guerts, S. Rau, W. Richter, and F. J. Schmitte, Thin Solid Films **121**, 217 (1984).
[22] F. Herman and F. Skillman, *Atomic Structure Calculations* (Prentice-Hall, Englewood Cliffs, NJ 1963).
[23] E. Clementi, D. L. Raimondi, and W. P. Reinhardt, J. Chem. Phys. **47**, 1300 (1967).
[24] P. C. Kemeny, J. Azoulay, M. Cardona, and L. Ley, Nuovo Cimento B **39**, 709 (1977).
[25] R. B. Shalvoy, G. B. Fisher, and P. J. Stiles, Phys. Rev. B **15**, 2021 (1977).
[26] P. C. Kemeny and M. Cardona, J. Phys. C **9**, 1361 (1976).
[27] S. A. Shivaji, U. K. Mohite, K. M. Gadave, and C. D. Lokhaande, Indian J. Pure Appl. Phys. **32**, 772 (1994).
[28] H. S. Soliman, D. A. A. Hady, K. F. A. Rahman, S. B. Youssef, and A. A. Elshazly, Physica A **216**, 77 (1995).
[29] J. Galy, G. Meunier, S. Andersson, and A. Aström, J. Solid State Chem. **13**, 142 (1975).
[30] R. J. Gillespie, *Molecular Geometry* (Van Nostrand Reinhold, London, 1972).
[31] A. Verbaere, R. Marchand, and M. Tournoux, J. Solid State Chem. **23**, 383 (1978).
[32] D. LeBallac, J. M. Kiat, and P. Garnier, J. Solid State Chem. **114**, 459 (1995).
[33] *Mössbauer Handbook Series: Tin-*^{119} *Handbook* (Mössbauer Effect Data Center, University of North Carolina, Asheville, 1990), and reference therein.
[34] J. R. Morton and K. F. Preston, J. Magn. Reson. **30**, 577 (1978).
[35] D. A. Shirley, Rev. Mod. Phys. **36**, 339 (1964).
[36] A. Svane and E. Antoncik, Phys. Rev. B **34**, 1944 (1986).